Helicopter rotor blade modal tuning using internal preloads

R. P. Dibble[1], B. Titurus[1]

[1] Department of Engineering, Queen's Building, University Walk, Bristol, BS8 1TR, United Kingdom

e-mail: **robert.dibble@bristol.ac.uk**

Abstract

There are many benefits of variable speed rotors if the associated dynamics problems can be alleviated. Existing passive and active methods are unsuitable due to their mass/power requirements and effectiveness over the necessary frequency range. The concept of inducing controlled 'stress softening' to alter the natural frequencies of a rotating structure in a vacuum and in turn avoid resonance is explored in this research. This paper presents an experimental and computational demonstration of this concept in the context of a small scale rotor blade representation. The model is successfully validated away from and within regions of coupling in which veering was present, and was therefore used to assess the effectiveness of the concept on full sized rotorcraft blades. Full scale assessment demonstrated that adequate separation can be achieved without requiring excessively large forces. The aim of the research is to create a semi-active method for the alteration of the blade's resonant frequencies to avoid resonance within a range of rotor speeds.

1 Introduction

The use of variable speed rotors offer considerable improvements to the performance of rotorcraft in terms of speed, noise, payload and range [1], [2]. However, the rotor's dynamics currently prohibit the alteration of rotor speed due to induced resonance.

The blade's natural and excitation frequencies are functions of rotor speed. Within a range of desired rotor speeds there will be many for which one of the blade's natural and excitation frequencies are similar. The proximity of these frequencies leads to resonance which will reduce fatigue life [3], decrease the levels of comfort for passengers, and have a detrimental effect on the reliability of the aircraft's sensitive mechanisms and equipment [4]. Traditionally, rotorcraft are designed to operate at a single rotor speed with blades that have been designed such that there is sufficient separation between the natural and driving frequencies.

Vibration suppression is of much interest to industry with work on a variety of active methods such as Higher Harmonic Control (HHC), Individual Blade Control (IBC) and active twist being completed. These systems are adaptable enough to operate over a range of frequencies, unlike Tuned Vibration Absorber (TVA) based passive systems, but have high mass/power requirements and are primarily designed for vibration reduction as opposed to resonance avoidance and therefore would not be suitable.

The concept of applying compressive loads to static structures to induce an effect known as 'stress softening' has been investigated [5], [6], [7]. The results [5] showed that a significant vibratory response reduction can be achieved over a range of frequencies using a single actuator. This project investigates the capability of structural preloading as a means to alter the natural frequencies of a rotating blade which would alleviate the dynamics problem associated with variable speed rotors. This method could provide an alternative method to avoid resonance in blades with a variable rotor speed. A system like this would be more adaptable than passive systems but without incurring the reliability or high power consumption issues inherent with active systems. This system could also be useful to avoid ground resonance or resonance during rotor spin up as well as during operational flight. As the majority of rotorcraft vibrations originate in the rotor, reducing these could also reduce the requirement for systems designed to reduce airframe vibration [4], [5], [8] such as Active Control of Structural Response (ACSR).

2 Methodology

2.1 Motivation

Centrifugal forces within a rotating rotor blade contribute to the restoring forces created when the blade is perturbed from equilibrium. The increase in restoring force increases the natural frequency, akin to an increased stiffness, and is therefore known as 'centrifugal stiffening'. A tensile loading of the blade would reduce these forces and therefore reduce the blade's natural frequency.

A suitably accurate model would provide insight into the suitability of the concept whilst highlighting any unexpected complexities that may be associated with it. Experimental data would be largely impractical to acquire and would include effects such as aerodynamics which may distort the effects of the preloading.

2.2 Mathematical model

Finite Element (FE) models are able to solve problems of great complexity but they were not used for the numerical model. A model based on the corresponding Boundary Value Problem (BVP) was chosen as it provided greater insight and intuition into the behavior of the system and the causes of it.

A constant cross section rotor blade attached to a uniform wire in a vacuum was modelled to test the concept. Simplicity was key for ease of validation and to ensure accuracy and understanding of the model. The effects of aerodynamics, damping, coupled degrees-of-freedom and hub/fuselage dynamics were omitted.

Due to rotor blade's high aspect ratios, see Figure 1, and the omission of aerodynamics, the blade was represented as a one dimensional structure. The blade's aspect ratio also ensures that planar sections would remain approximately plane and therefore Euler-Bernoulli beam formulation was used to write equations (1) and (2) [9]. The assumption of the blade tip harmonic transversal forcing allowed the time dependency to be removed from the equations. Flapping and lead-lag motions were both considered as these are the motions most influenced by centrifugal forces. The root of the blade is approximated as a point torsional and linear springs. A wire was used to apply preloading and as its dynamics would be dominated by its mass and the applied tensile load, not its stiffness, it was represented using the wave equation (3).

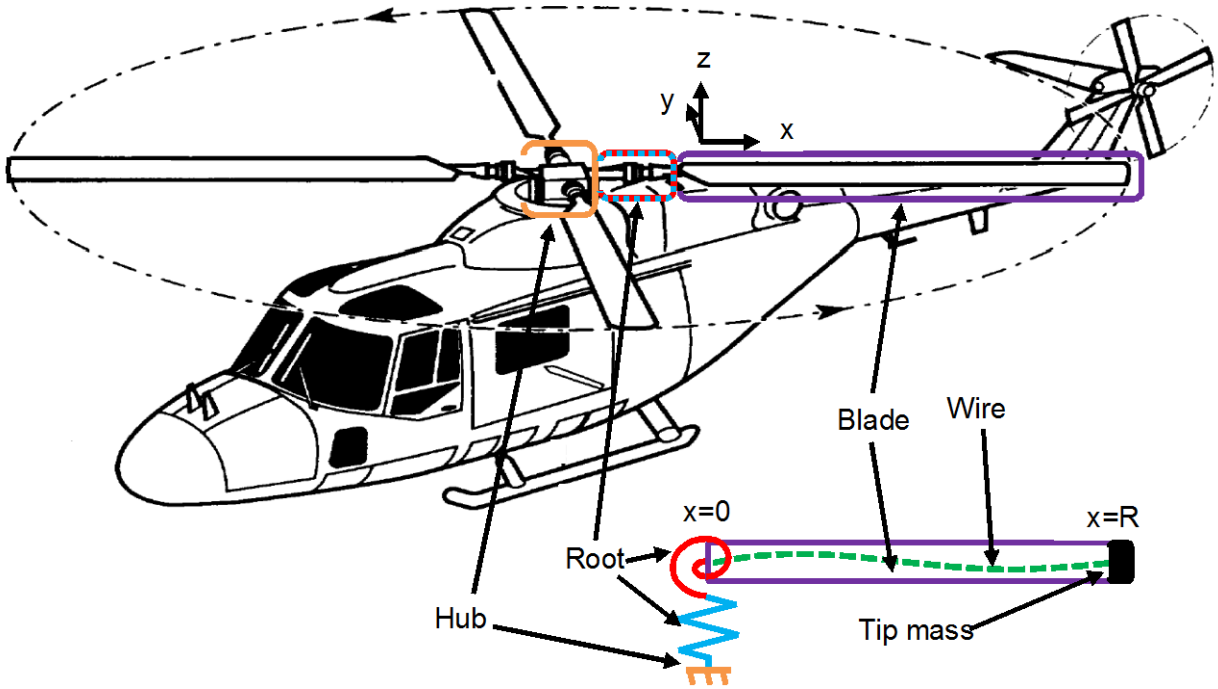

Figure 1: Helicopter sketch [10] and simplification of blade for modelling purposes

The blade flap, lead-lag and cable equations are specified as follows:

$$\frac{\partial^2}{\partial x^2}\left(EI_{flap}\frac{\partial^2 z}{\partial x^2}\right)-\frac{\partial}{\partial x}\left(T_b\frac{\partial z}{\partial x}\right)-m_b\omega^2 z=0 \tag{1}$$

$$\frac{\partial^2}{\partial x^2}\left(EI_{lag}\frac{\partial^2 y}{\partial x^2}\right)-\frac{\partial}{\partial x}\left(T_b\frac{\partial y}{\partial x}\right)-m_b\left(\omega^2+\Omega^2\right)y=0 \tag{2}$$

$$\frac{\partial^2 v}{\partial x^2}=-\frac{m_w}{T_w}\omega^2 v \tag{3}$$

Where $0\leq x\leq R$ is the domain of the blade; R is the length of the blade; EI is the stiffness constant in the direction of motion; z is the flapping displacement of the blade; y is the lag displacement of the blade; T_b is the tension in the blade; T_w is the tension in the wire; m_b is the linear density of the blade; m_w is the linear density of the wire; ω is the frequency of the motion; Ω is the rotor speed and v is the displacement of the wire.

Quasi-static tension forces in the beam and wire, equations (4) and (5), comprise of the applied tensile force, the centrifugal force of the tip mass and the centrifugal force due to the mass of the blade. It is assumed that the axial deformation of the wire and beam at the tip are equal.

$$T_w=F_{app}+T_{wtip}+\frac{1}{2}m_w\Omega^2\left(R^2-x^2\right) \tag{4}$$

$$T_b=-F_{app}+T_{btip}+\frac{1}{2}m_b\Omega^2\left(R^2-x^2\right) \tag{5}$$

Where F_{app} is the *applied* tensile force; T_{wtip} is the tension in the wire due to the tip mass and T_{btip} is the tension in the blade due to the tip mass.

To solve (1) and (2) *or* (1) and (3) as a BVP, six boundary conditions were required. For each boundary, the root and the tip of the blade, one moment, shear force equilibrium and wire-to-beam transversal displacement continuity conditions are used as seen in (6) to (11).

Assuming flapping motion of the rotating *coupled* blade-wire system, for the blade root where $x=0$

$$EI\frac{\partial^2 z}{\partial x^2}-K_t\frac{\partial z}{\partial x}=0 \tag{6}$$

$$T_w\frac{\partial v}{\partial x}+T_b\frac{\partial z}{\partial x}-EI\frac{\partial^3 z}{\partial x^3}-K_l z=0 \tag{7}$$

$$z-v=0 \tag{8}$$

and for the blade tip, $x=R$,

$$EI\frac{\partial^2 z}{\partial x^2}=0 \tag{9}$$

$$F_0-T_w\frac{\partial v}{\partial x}-T_b\frac{\partial z}{\partial x}+M_{tip}\omega^2 z+EI\frac{\partial^3 z}{\partial x^3}=0 \tag{10}$$

$$z-v=0 \tag{11}$$

Where K_t is the root torsional stiffness; K_l is the root linear stiffness and M_{tip} is the mass of the tip mass. F_0 is the magnitude of *applied* harmonic excitation. Equivalent boundary conditions were derived and used for the lead-lag motion. All subsequent computational studies were completed for the condition where $M_{tip}=0$.

2.3 Solution process

Receptance Frequency Response Functions (FRFs) were created by performing a computational sine sweep on the system described in the previous section. A range of values for ω were swept through and the response of the system at that excitation frequency was recorded. This technique allowed for the creation of FRFs which could then be compared to the experimental equivalents if necessary. As the assumption of harmonic motion allowed for the time dependency of the initial model to be removed, the system was represented as a set of higher order Ordinary Differential Equations (ODEs) with boundary conditions to be met at the extremes of the domain. The system was therefore treated as Boundary Value Problem and solved using the collocation method. Collocation uses a finite-dimensional space of potential solutions and a number of points in the domain (collocation points) to select the solution which satisfies the equation at these points. A collocation solver [11] implemented in MatLab (R2015a) was used for this analysis.

3 Experiment-based case study

An experimental case study was performed to highlight any discrepancies and errors between the model and experiment as well as to assess the accuracy and therefore validity of the modelling techniques used. Due to practical limitations a non-rotating experiment was performed on a mock blade and root configuration with the first three bending modes being analysed.

3.1 Test structure

A mock blade and root configuration with attached wire was setup to represent the configuration used in the model, see Figure 1. The primary component consisted of a thin walled aluminium beam with rectangular cross section which was used to represent the blade. The beam had a thickness to chord ratio of 0.51 and an aspect ratio of 39.2, as seen in Figure 2, to replicate the dynamics of a rotor blade as closely as possible. One end of this beam was attached to a short, thin, steel beam, which in turn was tightly clamped to the bench. This shorter beam represented the hinge section and hub attachment that is present in full sized aircraft. At the free end of the main beam there was an insert used to hold the wire in place. The 1.8 mm diameter steel wire ran from the attachment point at the tip, through the inside of the beam, through a hole in the root beam, over a pulley and was then attached to a mass hanger. The amount of mass placed on the hanger was controlled to determine the amount of preloading in the structure. The beam was mounted such that the motion of the tip was horizontal to minimise gravitationally induced effects.

An accelerometer and impact hammer were used to perform modal analysis on a range of preloading configurations. Excitation and measurement were both performed at the tip of the beam to give point FRFs. The tip is a location at which a modal node shall never be present which ensures all desired modes were captured. A brief experiment using a range of measurement and excitation locations concluded the same result. The maximum sampling rate of 2048 Hz was used as this resulted in a Nyquist frequency of 1024 Hz which was higher than the range of frequencies studied and therefore eliminated potential aliasing. A 30 second sampling window was used as this was sufficient to acquire low noise data with no leakage. Eight repetitions were performed, with anomalous results repeated, and the mean FRFs calculated for further use.

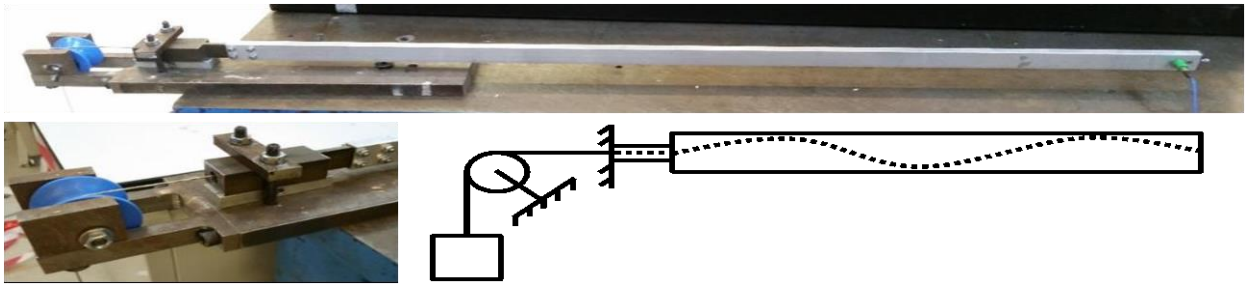

Figure 2: Experimental configuration

3.2 Unloaded reference model validation and parameter identification

The accurate calculation of the properties of the experiment were essential to ensure that the experimental and computational results correlated well. The linear density properties, mass properties and geometric properties were easily measured. The values for EI, K_t and K_l were identified using both static structural tests and dynamic tests and were compared to ensure accuracy. The structural tests consisted of a three point bend test of the isolated beam to calculate EI, and a moment-displacement test to calculate K_t which was then used to calculate K_l using beam theory. For the dynamic tests a free-free experiment was performed on the isolated beam and an equivalent FE model was used to calculate EI such that the error between the FE model and the free-free experiment was minimized for the first and third mode. To calculate K_l and K_t an experiment was performed to acquire the first three modes of the beam and root configuration without the wire or tip mass. An FE model that calculated K_l and K_t directly such that the error in the first three modes was minimized was one method for acquiring K_l and K_t. The other method used an FE model to calculate EI of the short root section and beam theory to calculate K_l and K_t from this.

A reference model with no wire (the omission of (3), (8), (11) and the associated terms in the remaining boundary conditions) was used to compare the natural frequencies created using these parameters with the experimental ones of the configuration with tip mass but no wire. The values using structurally calculated parameters were closest to the experimental ones across all three modes and therefore it was these parameters, show in Table 1, which were chosen for the validation of the full model. It was observed that the differing sets of parameters produced a large variation in calculated spring stiffnesses. This is likely to be because the root is so stiff that the system is nearly cantilevered and therefore relatively insensitive to changes in these parameters.

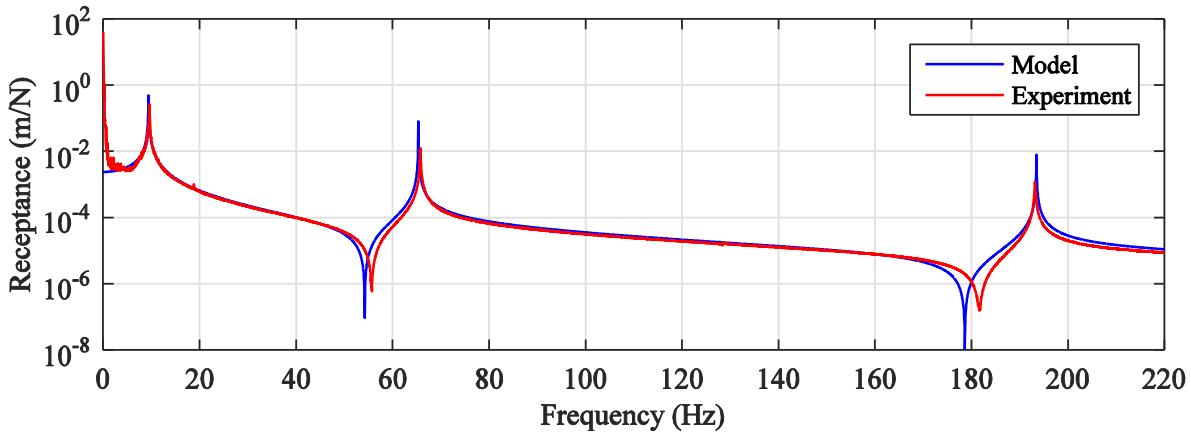

Figure 3: Comparison of experimental and modelled FRFs

	Structural
R (m)	0.998
m_b (kg/m)	0.281
EI (Nm^2)	168.88
K_t (Nm/rad)	2.4017 x10^3
K_l (N/m)	1.1547 x10^7

Table 1: Summary of reference model parameters

The low error across the three modes (-1.90%, -0.68% and 0.10% respectively) indicates that the model and the parameter values calculated provide a satisfactory representation of the experimental structure. The assumptions of constant properties and point mass and springs appear valid and there is sufficient confidence in the model to proceed with the validation.

3.3 Coupled beam-cable model validation

Results from the full model (with wire) were compared with the experimental results to assess the model's ability to capture the influences of the wire. The experimental FRFs were stacked adjacently and viewed from above to allow for easy tracking of the changes in FRF peaks as the preloading was varied, Figure 4.

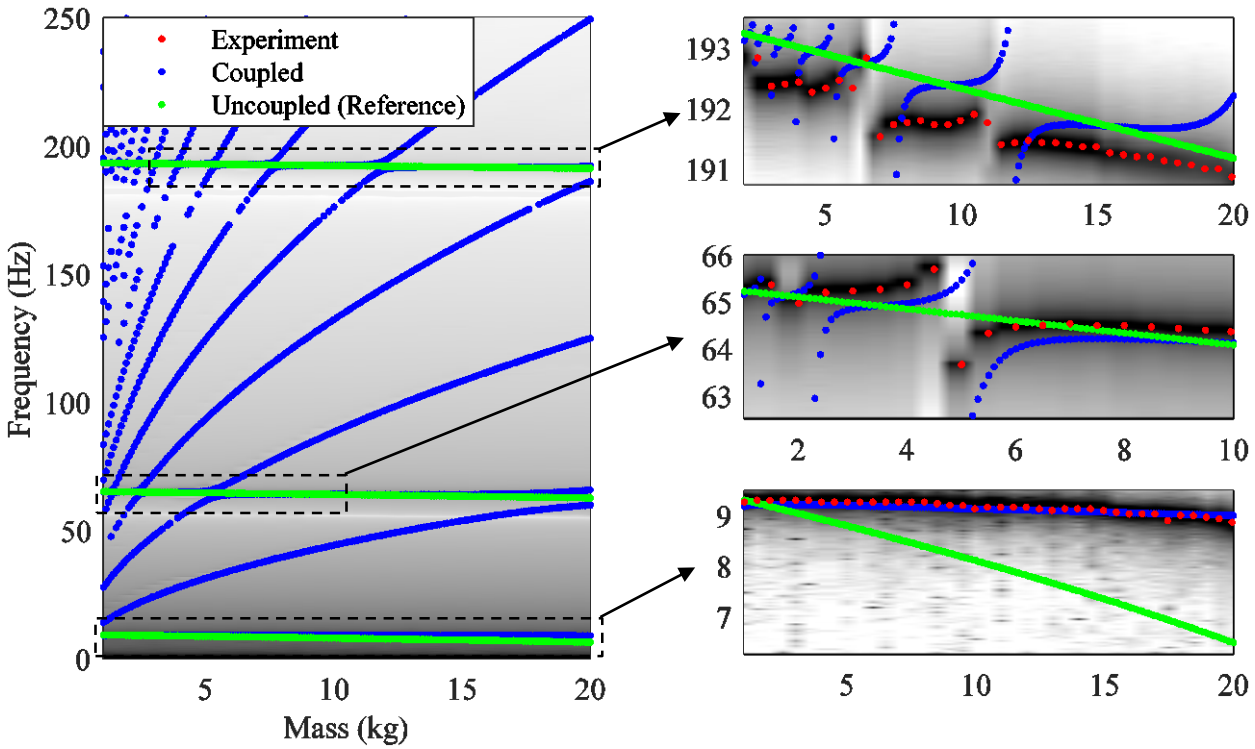

Figure 4: FRF peaks from coupled and reference model overlaid on the experimental data (black colour represent large responses and white color represent small response)

Figure 4 shows that the reference or uncoupled model (no wire, $F_{app}\neq 0$) captures the decrease in resonant frequencies that is the general trend shown in the experimental data but overestimates the rate of decrease in the lower modes. The coupled model (wire included, $F_{app}\neq 0$) represents the first and second FRF peak variation well in terms of its shape and the accuracy of the values but loses accuracy near the third FRF peak. As it has the same shape it is expected that the discrepancy (~0.5%) is due to inaccuracies in the properties of the beam and wire or unmodelled effects such as damping or friction.

Due to the good correlation, even within the regions of the beam-wire interaction, the coupled model was deemed valid for a stationary case. Due to practical limitations an equivalent experiment to validate the model for a rotating case could not be performed. However the model did show the expected increase in natural frequencies with rotor speed and therefore the model was used for rotating cases. Due to observed and assumed low damping in the studied system, FRF peaks will be associated with the modal or natural frequencies of the system in the rest of the paper.

3.4 Wire beam interaction

It can be seen in Figure 4 that there is a strong coupling effect present in regions where the beam and wire appear as if they should cross. This effect is particularly noticeable at ~65 Hz with a loading of ~5 kg; where the second beam and second wire mode interact. The experiment was therefore repeated between 4.5 kg and 5.5 kg with 0.1 kg increments to provide more detail on this region of coupling, Figure 5.

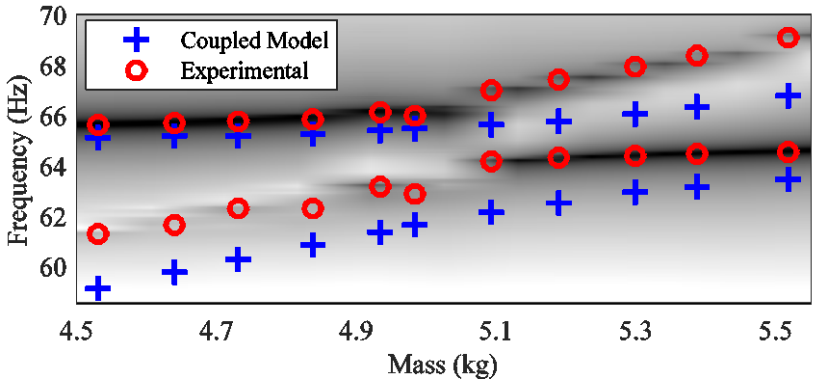

Figure 5: Experimental and modelled response variation during coupling

It can be seen in both the experimental and modelled results that the beam and wire modes appear to be on trajectories to intersect but move away from each other as they approach the point of intersection. This phenomenon, known as *veering*, is also characterised by the modes switching so that after the interaction they each follow the path that the other was previously on with the associated modeshape of that mode; almost as if they had crossed [12]. For example, the lower of the two modes is originally a wire mode but has changed to a beam mode after the interaction; with the opposite being true for the higher mode.

The model is not only able to predict behavior of the change in the natural frequencies associated with veering, albeit imprecisely, but it also demonstrates the expect change in modeshapes across the interaction. Figure 6 shows the modeshapes of the model across the aforementioned interaction.

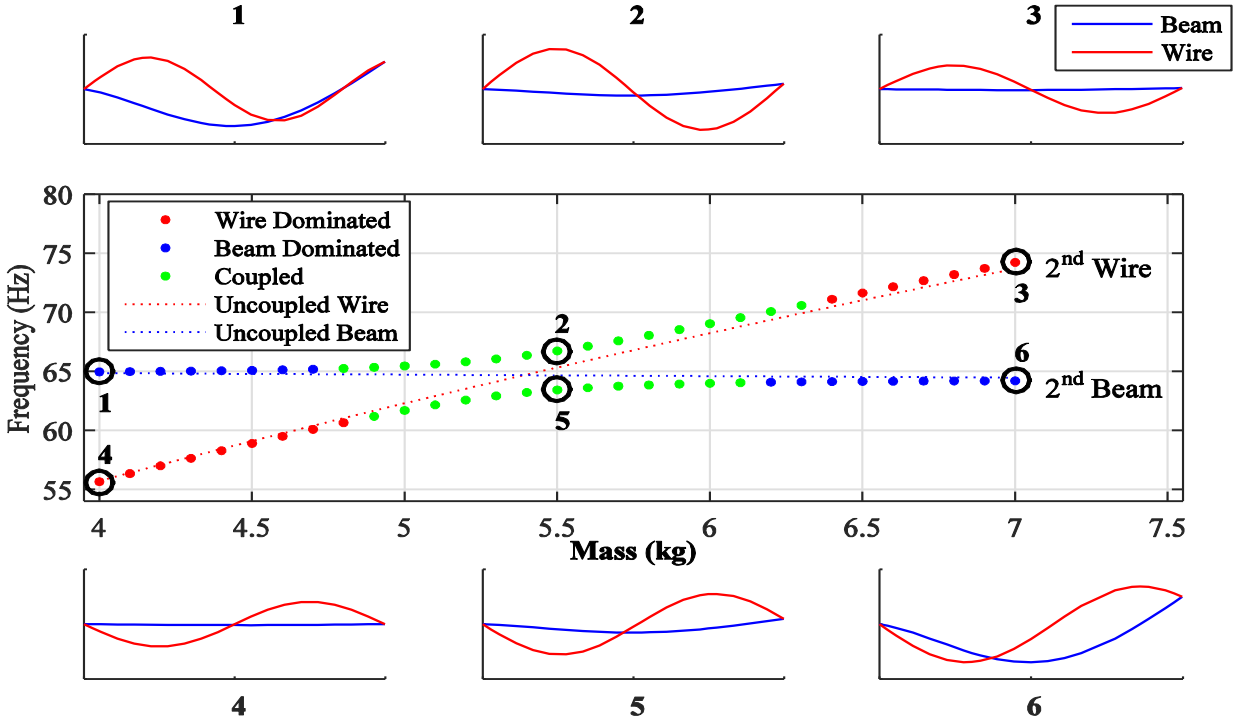

Figure 6: Variation of the system's natural frequencies, which element they are dominated by and the variation of the modeshapes.

It can be seen in Figure 6 that there is notable similarity between the mode shapes in 1 and 6; and 3 and 4 which confirms the presence of veering and the ability of the model to predict it. In these regions of coupling the natural frequencies of the beam and wire would be equal if they were not coupled, therefore the wire could be treated as a TVA which, due to its tension, has been tuned to the beam's natural frequency. Although the regions in which this is effective are far smaller than the primary concept of altering the blade's natural frequency, due to its ability to create a large change in natural frequency it may be beneficial to employ this phenomenon to improve the system's effectiveness.

4 Model-based case study

4.1 Model parameters

Once validated, the model could be used to investigate the effects and sensitivities of various parameters on the concept. Of particular interest is the behavior of the concept when parameters are representative of full sized rotorcraft. The MBB Bo 105 and Westland Lynx have significantly different capabilities, as seen in Table 2. These different design specifications result in significantly differing blade properties, in particular specific stiffness and length, therefore these aircraft were chosen for comparison.

The distributed mass and stiffness properties of the blade were averaged for use in the model and beam theory was used to calculate the point spring equivalents of the root sections. The linear density of the wire was calculated using Nickel-Cr-Co-Mo alloy due to its high specific fatigue strength, and sized such that it could withstand the required tension force without exceeding the fatigue stress. This removes the fatigue problems which would trouble a component that would be subjected to a large number of cycles.

	Aircraft A: MBB Bo 105 [13][14]	**Aircraft B: Lynx** [10][15]
Sector	Civilian	Military
Mass (kg)	2500	5330
Passengers	4	8
Max speed (km/h)	242	324
Rotor diameter (m)	9.82	12.80
Ω_0 (rad/s)	44.5	33.3
EI_{flap} (kNm^2)	7.20	45.8
EI_{lag} (kNm^2)	164	503
m_b (kg/m)	7.27	7.14
$K_{t,flap}$ (Nm/rad)	2.47×10^6	1.19×10^5
$K_{l,flap}$ (N/m)	2.59×10^8	1.70×10^6
$K_{t,lag}$ (Nm/rad)	3.08×10^6	1.19×10^5
$K_{l,lag}$ (N/m)	3.23×10^8	1.70×10^6

Table 2: Summary of specifications of aircraft to be modelled

4.2 Sensitivity analysis

The uncoupled reference model was initially run for stationary blades to assess whether the concept worked on full scale blades under similar conditions to that of the experiment. The uncoupled model was chosen as it ensures the preloading effects are captured, not the wire interactions. Figure 7 shows that the expected effect of reducing the natural frequency can be observed in all natural frequencies of both motions of both aircraft.

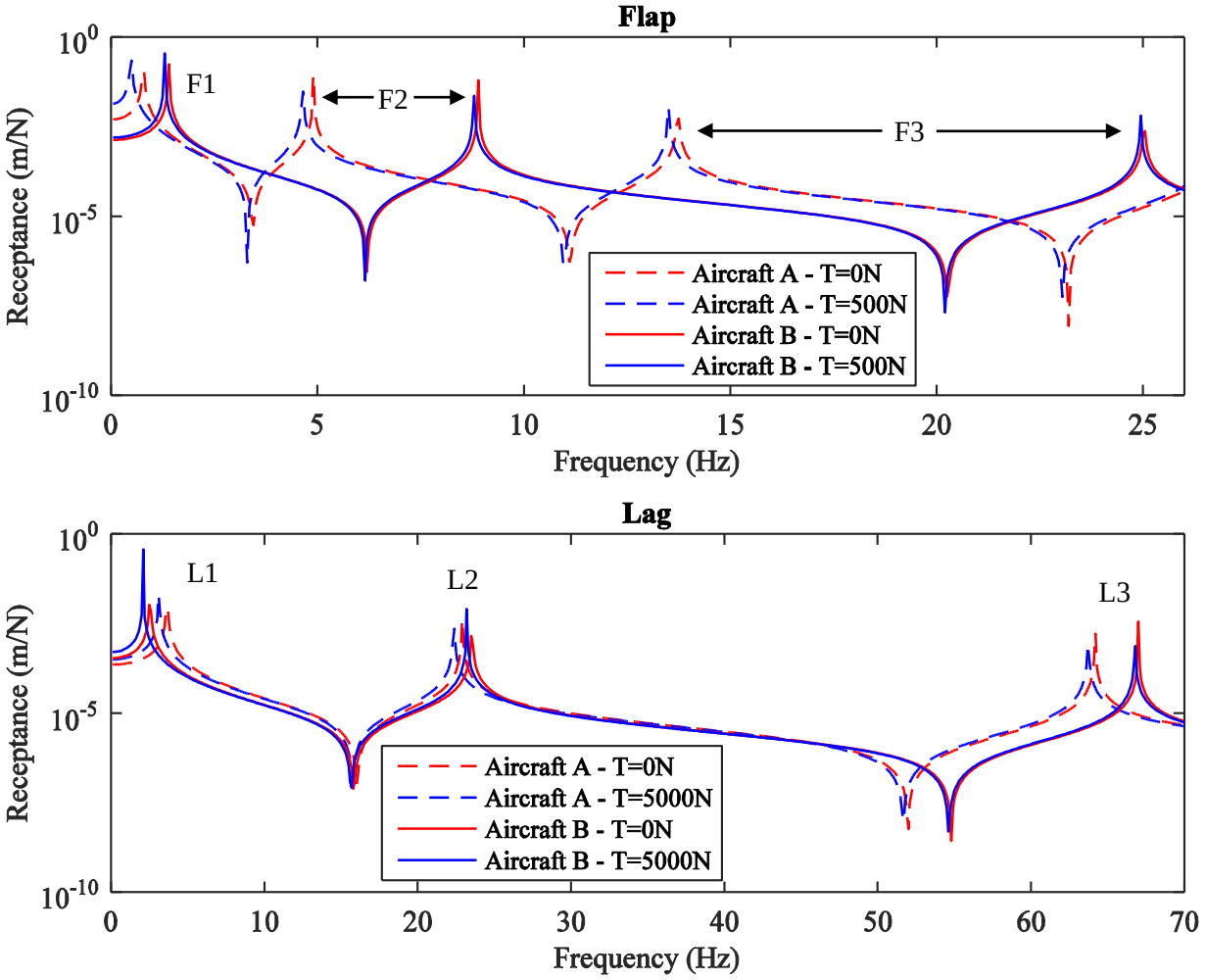

Figure 7: FRFs for the Flap and Lag motions of Aircraft A and B with and without preloading at Ω=0

The uncoupled reference model was then used to investigate the effect of rotation on the concept's ability to alter natural frequencies. The absolute values on the left hand side of Figure 8 show that the rotating blade has higher frequencies, which is expected due to centrifugal stiffening. It can also be seen that at the prescribed preloadings the non-rotating blade would have buckled as its fundamental frequency would have reached zero. The normalised values on the right hand side of Figure 8 highlight the sensitivity of each of the modes. Zhang *et al* [16] demonstrated that the sensitivity of a beam's frequencies to axial loading increased as the loading approached the critical buckling case. All of the modes show this trend of increasing sensitivity with the axial load and it is most evident in the non-rotating fundamental modes as they have the lowest critical buckling load. Whilst it can be observed that there is a tighter grouping between all three modes for the rotating lag case than in the rotating flap case, there is significant disparity between which modes or type of motion is the most sensitive. This is true for both the rotating and non-rotating cases.

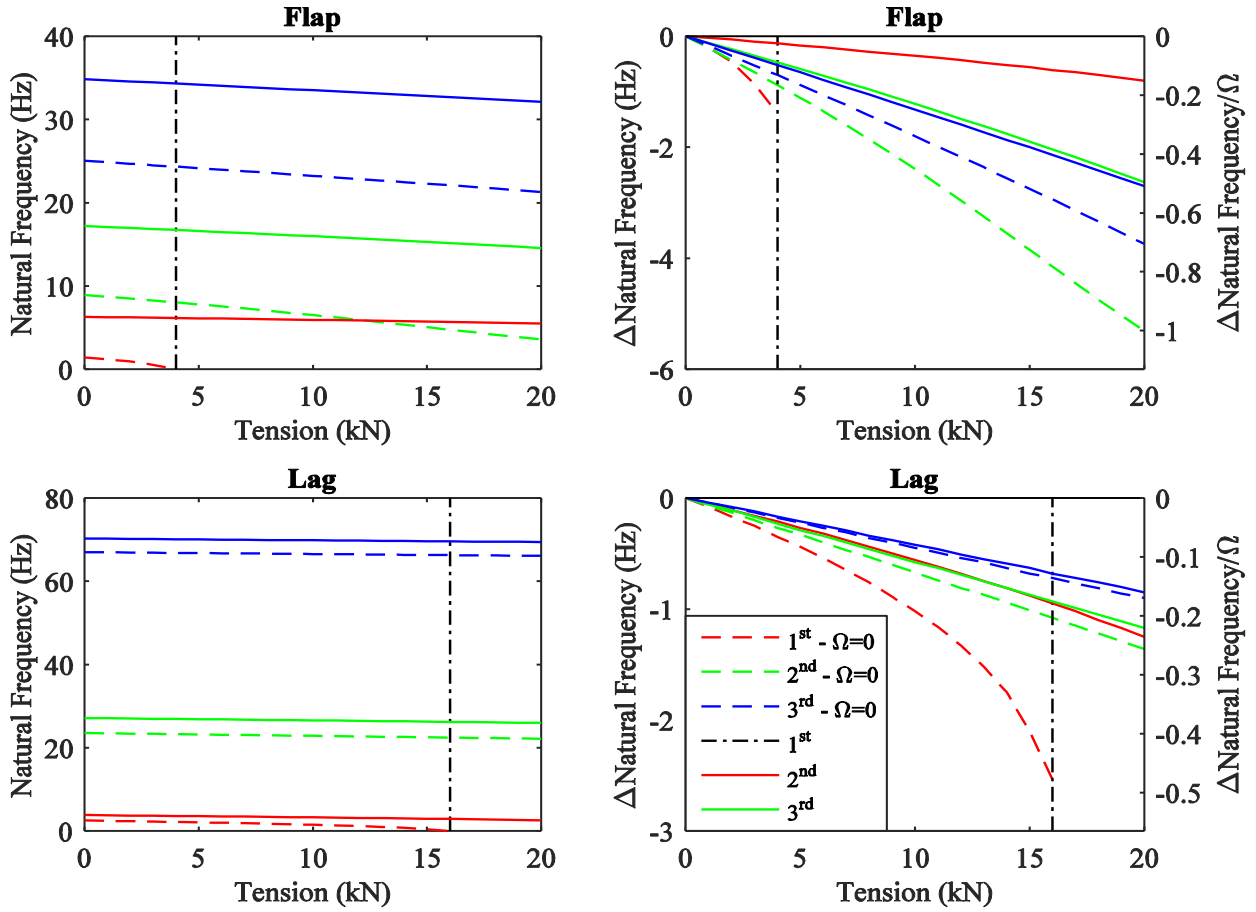

Figure 8: Effect of rotation on frequency alteration

Another sensitivity study was performed on the fully coupled model to assess the effects of the wire's mass, as seen in Figure 9. Similarly to Figure 5 this study was focused around the second bending mode.

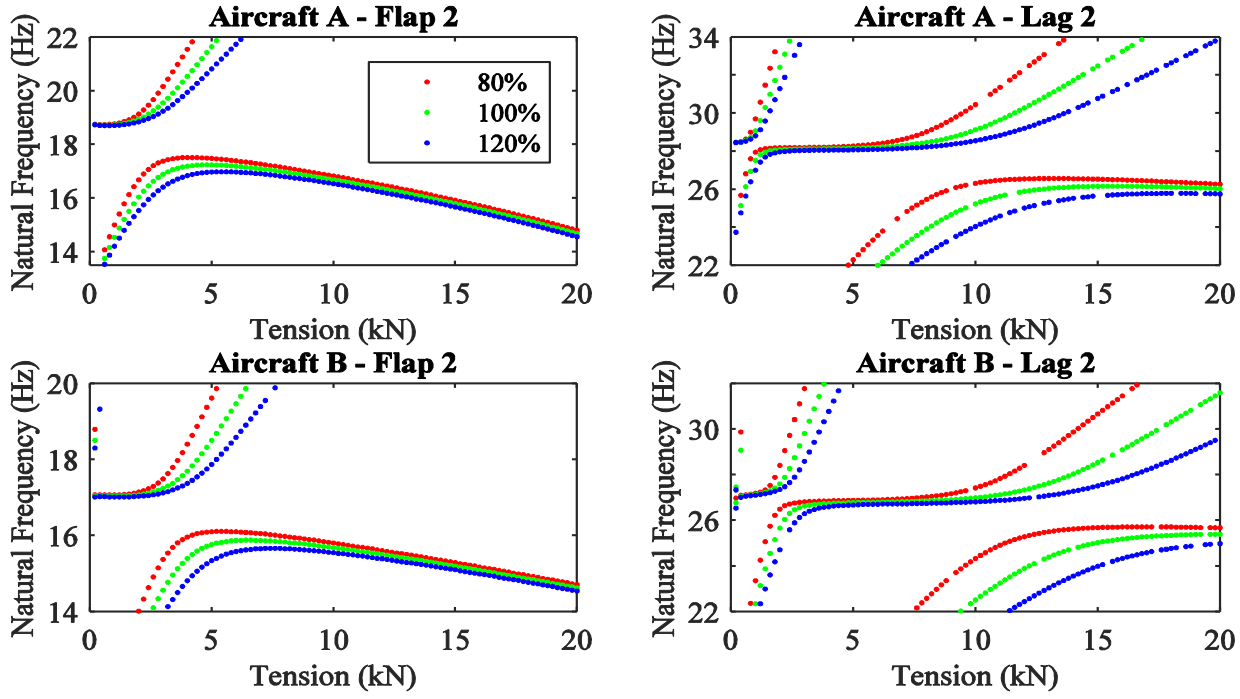

Figure 9: Variation in wire-beam interactions with changing wire mass

Away from regions of interaction the effects are as expected; the wire's frequencies change drastically and the beam's are unaffected. However in regions of coupling there is a considerable change. As the mass of the wire increases, becoming closer to the mass of the beam, the region coupling increases and the transition from the system being dominated by the beam or wire is far smoother.

4.3 Results for full scale application

It is recommended that the margin between the natural frequencies of a blade and the driving frequencies is 10% of the rotor frequency [17]; therefore if a frequency is 10% above then the *reduction* in frequency required will be 20% of the rotor frequency. The fundamental flap mode is heavily aerodynamically damped and the fundamental lag mode is usually far lower than the lowest excitation frequency and therefore these modes shall be omitted from the assessment. The second modes are used as the critical case because they will interact with the lower driving frequencies which have more energy. The fully coupled model was then used to assess these modes and their variation with preloading for a range of rotor speeds, as seen in Figure 10.

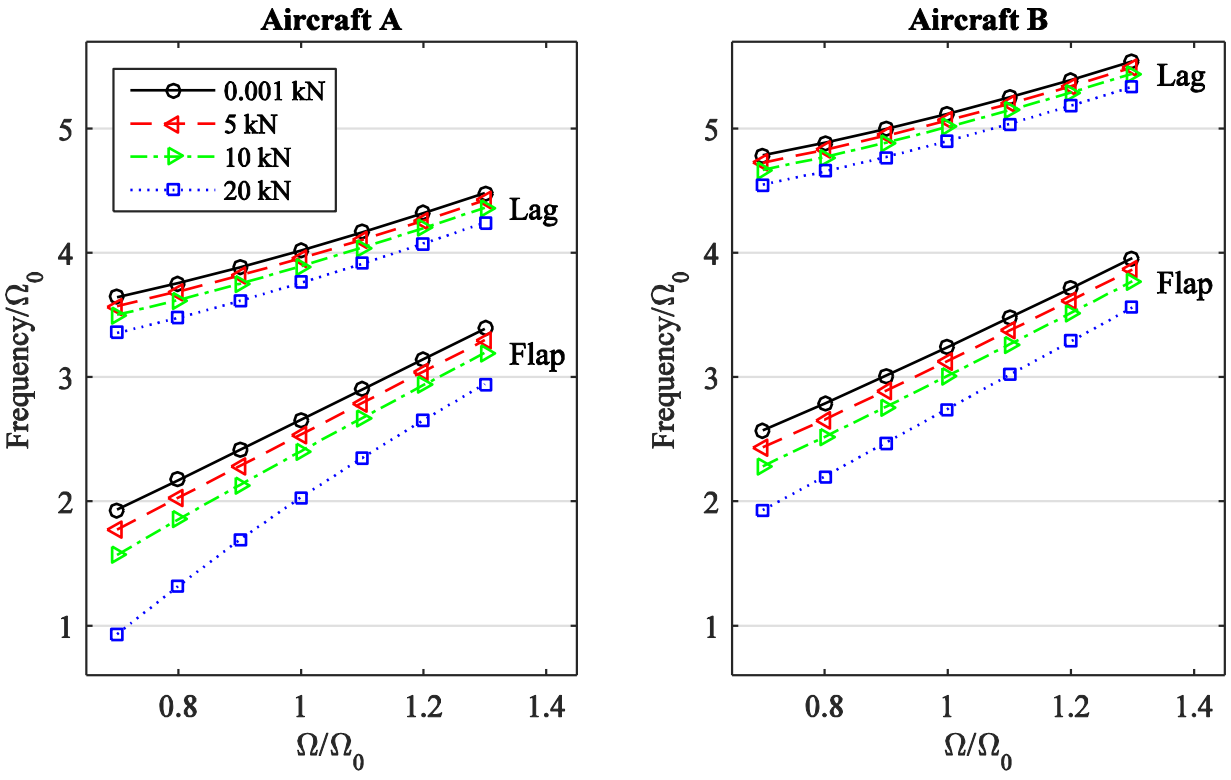

Figure 10: Variation in second flap and lag mode of blade with changing rotor speed and preloading

It can be seen that for both aircraft the flap modes are more sensitive than the lag modes and that all of the modes appear to be more sensitive at lower rotational frequencies. Aircraft A also appears to be more sensitive than Aircraft B, despite its higher rotor speed. This is particularly noticeable in the flap mode, which may be due to its comparatively low stiffness.

For the aforementioned reasons the second lag mode was used as the critical case to analyse the required applied tensile loads to achieve the required shift in natural frequency, results of which have been summarized in Table 3. It can be seen that the required forces are lower when using the coupled model compared to the uncoupled model. This is because the inclusions of the wire's dynamics have allowed the natural frequencies to be increased, and as the analysis was configured for the frequency to be on the upper limit, only a small increase is required to achieve sufficient separation. Furthermore the inclusion of the wire's dynamics allow the previously discussed TVA effects to be employed. Again, only a relatively small

amount of tension is required to tune the antiresonance created to that of the driving frequency. In both situations with the coupled model it should be noted that the effect of the wire will decrease drastically away from regions of coupling and therefore the effect of the changes in natural frequency will differ greatly between modes.

Although these forces may appear large they will not induce buckling in the blade. As seen in Figure 8 the model is capable of predicting buckling (dash-dotted line) but due to the centrifugal forces being orders of magnitude higher than the tensile load, the majority of the blade remains in tension and therefore buckling is not present. Whilst not currently assessing actuation methods it should be noted that actuators capable of 10kN weigh ~3kg and require ~300W. Furthermore the mass of the wire would add only a small amount of mass to the blade, even when sized conservatively for the larger forces required by the uncoupled model.

	Aircraft A	**Aircraft B**
Original frequency (Hz)	28.47	27.16
Required frequency change (Hz)	1.42	1.06
Force required – Uncoupled (kN)	15.5	18.2
Force required – Coupled (kN)	4.9	6.8
Force required – TVA Tuned (kN)	6.7	8.7
m_w/m_b (%) – Uncoupled	1.72	1.75

Table 3: Summary of blade alteration values

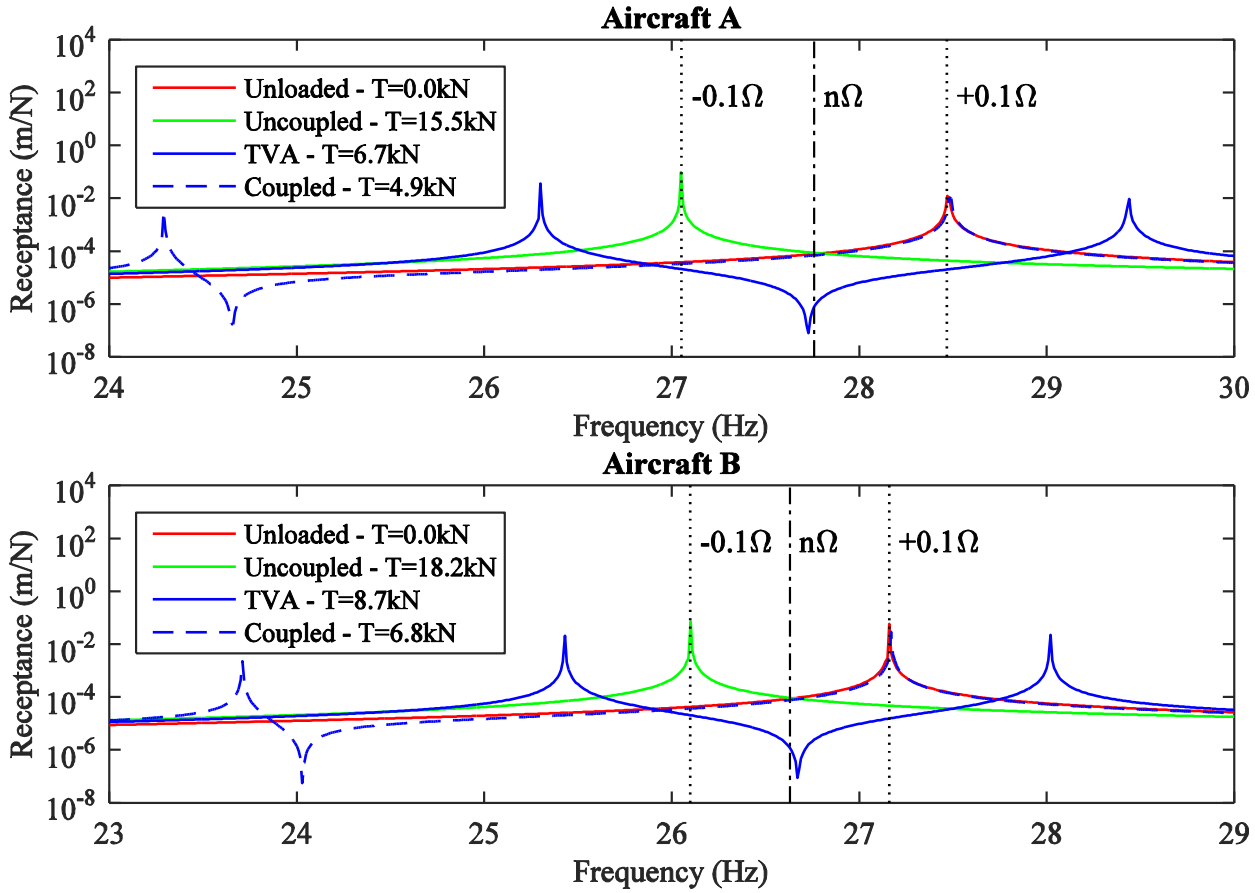

Figure 11: FRFs of second lag mode to achieve adequate separation

5 Conclusion

The concept has been successfully demonstrated both experimentally and mathematically. Although unvalidated for non-stationary blades, the required tensile loads predicted by the models for sufficient separation are low enough that they could be realistically achieved without an actuation system that is so heavy that it would negate the benefits of variable speed rotors.

The sensitivity of the blade's natural frequencies to preloading varied drastically with variation in motion type, rotor speed, stiffness and modal order when studied using the uncoupled model. The coupled model demonstrates that separation can be achieved either by applying preloading such that blade's natural frequencies reduce sufficiently *or* by tuning the wire as if it were a TVA.

Thus far each motion type has been considered whilst coupled with the wire but uncoupled from each other. Whilst the concept has been demonstrated to work on both motions the more complex nature of a fully coupled flap, lag and twist rotor blade must also be considered. Alongside this an equivalent experiment must be performed to allow for sufficient validation. A model of this nature would capture the coupling between the various motions and the wire itself, allowing a more realistic assessment of the system's ability to ensure separation of all resonances of a range of rotor speeds.

Acknowledgements

The author would like to thank The University of Bristol, The UK Vertical Lift Network and ESPRC for their guidance and funding, without which this research would not have been possible.

References

[1] M. Allongue, H. Marze, F. Potdevin, *Quiet Helicopter 'from research to reality'*, in *American Helicopter Society - Annual Forum Proceedings, Montreal, 1999*.

[2] A. E. Karem, *OPTIMUM SPEED ROTOR*. United States Patent 6,007,298, 28 December 1999.

[3] J. W. v. Wingerden, A. Hulskamp, T. Barlas, I. Houtzager, H. Bersee, G. v. Kuik, M. Verhaegen, *Two-Degree-of-Freedom Active Vibration Control of a Prototyped "Smart" Rotor*, IEEE TRANSACTIONS ON CONTROL SYSTEMS TECHNOLOGY, vol. 19, no. 2, pp. 284-296, 2010.

[4] J. Pearson, R. Goodall, I. Lyndon, *Active Control of Helicopter Vibration*, Computing Control Engineering Journal, vol. 5, no. 6, pp. 277-284, 1994.

[5] J. D. Bois, N. Lieven, S. Adhikari, *Adaptive Passive Control of Dynamic Response through Structural Loading*, in *48th AIAA/ASME/ASCE/AHS/ASC Structures, Structural Dynamics and Materials Conference, Honolulu, 2007*.

[6] T. Turkstra, S. Semercigil, *Elimination of Resonance with a Switching Tensile Support*, Journal of Sound and Vibration, vol. 163, no. 2, pp. 359-362, 1993.

[7] M. L. Chen, Y. S. Liao, *Vibrations of pretwisted spinning beams under axial compressive loads with elastic constraints*, Journal of Sound and Vibration, vol. 147, no. 3, pp. 497-513, 1991.

[8] P. Konstanzer, B. Enenkl, P. Aubourg, P. Cranga, *Recent advances in eurocopter's passive and active vibration control*, in *American Helicopter Society 64th Annual Forum, Alexandria, 2008*.

[9] G. Done, D. Bramwell, *Bramwell's Helicopter Dynamics*, Butterworth Heinemann, 2001.

[10] B. H. Lau, A. W. Louie, N. Griffiths, C. P. Sotiriou, *Performance and rotor loads measurements of the Lynx XZ170 helicopter with rectangular blades*, 1993.

[11] L. F. Shampine, J. Kierzenka, M. Reichelt, *Solving Boundary Value Problems for Ordinary Differential Equations in MATLAB with bvp4c*, Natick, MA: The Mathworks, Inc, 2000.

[12] J. L. d. Bois, S. Adhikari, N. A. Lieven, *Eigenvalue curve veering in stressed structures: An experimental study*, Journal of Sound and Vibration, vol. 322, pp. 1117-1124, 2009.

[13] J. A. Staley, *Validation of Rotorcraft Flight Simulation Program through Correlation with Flight Data for Soft-in-Plane Hingeless Rotors*, AMRDL, 1976.

[14] J. W. Taylor, *Jane's All the World's Aircraft*, Jane's Information Group, 1988-1989.

[15] M. J. Taylor, *World Aircraft & Systems Directory*, Flight International, 2001.

[16] Y. Q. Zhang, Y. Lu, S. L. Wang, X. Liu, *Vibration and buckling of a double-beam system under compressive axial loading*, Journal of Sound and Vibration, vol. 318, pp. 341-352, 2008.

[17] Agusta Westland, Guidance Notes on Main Rotor Design, 2013.